AIP | The Journal of Chemical Physics

# An assessment of mean-field mixed semiclassical approaches: Equilibrium populations and algorithm stability

Nicole Bellonzi, Amber Jain, and Joseph E. Subotnik

Citation: The Journal of Chemical Physics **144**, 154110 (2016); doi: 10.1063/1.4946810
View online: http://dx.doi.org/10.1063/1.4946810
View Table of Contents: http://scitation.aip.org/content/aip/journal/jcp/144/15?ver=pdfcov
Published by the AIP Publishing



# An assessment of mean-field mixed semiclassical approaches: Equilibrium populations and algorithm stability

Nicole Bellonzi, Amber Jain, and Joseph E. Subotnik
*Department of Chemistry, University of Pennsylvania, Philadelphia, Pennsylvania 19104, USA*

(Received 7 January 2016; accepted 24 March 2016; published online 21 April 2016)

We study several recent mean-field semiclassical dynamics methods, focusing on the ability to recover detailed balance for long time (equilibrium) populations. We focus especially on Miller and Cotton's [J. Phys. Chem. A **117**, 7190 (2013)] suggestion to include both zero point electronic energy and windowing on top of Ehrenfest dynamics. We investigate three regimes: harmonic surfaces with weak electronic coupling, harmonic surfaces with strong electronic coupling, and anharmonic surfaces with weak electronic coupling. In most cases, recent additions to Ehrenfest dynamics are a strong improvement upon mean-field theory. However, for methods that include zero point electronic energy, we show that anharmonic potential energy surfaces often lead to numerical instabilities, as caused by negative populations and forces. We also show that, though the effect of negative forces can appear hidden in harmonic systems, the resulting equilibrium limits do remain dependent on any windowing and zero point energy parameters. *Published by AIP Publishing.* [http://dx.doi.org/10.1063/1.4946810]

## I. INTRODUCTION

Modeling photoexcited dynamics is a very difficult endeavor. Besides the obvious problem of electronic structure, there is the separate issue of how to propagate nuclear dynamics on more than one potential energy surface (PES). After all, with many nuclei, propagating exact quantum dynamics on even one adiabatic surface is exponentially expensive for large systems. In practice, mixed quantum-classical methods are the only possible approaches that can handle atomic systems.

Within the realm of semiclassical mechanics, there are a host of different mixed quantum-classical nonadiabatic approaches, some based on stochastic approaches,[1–3] some based on spawning,[4,5] some based on master equations,[6–8] and many based on mean-field theories.[9–12] The reason for such a diversity of approaches is the fact that there is no unique way to embed quantum mechanics inside of classical mechanics; there is no one unique approximation for reducing a subset of quantum degrees of freedom to classical degrees of freedom while conserving all necessary symmetries of the universe.

Historically, perhaps the most famous approach is the quantum classical Louiville equation (QCLE). The QCLE is derived[13–17] by first performing a Wigner transform of the nuclear degrees of freedom and then cutting off the nuclear equation of motion at order $\hbar$. The resulting QCLE satisfies most necessary symmetries (but not all, e.g., the time translation of equilibrium averages[18]). The QCLE is exact for linearly coupled, harmonic (i.e., spin-boson) systems and can be quite accurate for nonlinear, nonharmonic systems.[15] In general, the deterrent for using the QCLE is that the QCLE incorporates a set of notoriously unstable partial different equations which can preclude any easy implementation.[19,20]

Apart from the QCLE, surface hopping[1,21] and Ehrenfest (mean-field) dynamics[9,22] are two broad classes of approaches that aim to correctly model nonadiabatic dynamics while remaining computationally affordable. Omitting many details that will be discussed later, surface hopping propagates dynamics along a single adiabatic PES while allowing hops between PESs; mean-field dynamics propagate dynamics along an averaged PES. In the first case, quantum effects are embedded in the hops, while in the second case, quantum effects are taken into account by movement along an average PES (that changes dynamically in time).

Now, although Ehrenfest dynamics were suggested long ago, in recent years there have been a few new algorithms that effectively aim to improve Ehrenfest dynamics. These new algorithms have been derived through different means, but their conclusions are similar. On one hand, Ehrenfest-like dynamics can be derived by using the famous Meyer-Miller-Stock-Thoss (MMST) transformation,[23–26] whereby one bosonizes the electronic degrees of freedom. Subsequently, one can apply either straightforward classical mechanics[23] or linearized semiclassical theory. On the other hand, as shown by Kapral, these same dynamics can be derived by considering the QCLE in the MMST basis and ignoring a cubic term. For simplicity, we will denote these dynamics Poisson-Bracket Mapping Equation (PBME) dynamics below.[11,12,27] As discussed below, PBME is different from Ehrenfest dynamics only in so far as how exactly the average force is computed, how one chooses the initial conditions (with or without zero point energy), and how exactly one defines a population later on time. That being said, the structures of both algorithms are extremely similar. For details of these methods, and further analysis, see below as well as Refs. 11 and 27–30.

More recently, a second approach to improving Ehrenfest dynamics was implemented by Miller and Cotton,[31] entitled "symmetrical quasi-classical windowing" (SQC). The basic premise of SQC (as suggested long ago[67]) is to symmetrically window both the initial and final trajectories (in the spirit of a quasi-classical vibrational analysis[32,33]) so as to include

some zero point energy and also make sure that only physical trajectories (with near integer quantum values) are counted in any averaging. The initial conditions and average force for SQC are essentially the same as for PBME; see below for precise details. Preliminary results for this method have been encouraging.[10,31,68] However, several different variations of SQC can be formulated and a complete systematic testing has not yet been published.

With this history in mind, the goal of the present article is to analyze the mixed quantum-classical, mean-field approaches described above, first framing each algorithm within a single, consistent framework and second making a comparative benchmark of the resulting dynamics. Whereas many of these algorithms have previously been scrutinized for their short time dynamics,[34] our primary concern will be the ability to recover the correct long-time, equilibrium populations that satisfy detailed balance.[35,36] Without such capability, statistical analyses will certainly be challenging.

Let us consider the simplest case of two weakly coupled electronic states. For such a case, the correct populations must satisfy Boltzmann statistics,

$$\frac{P_1}{P_2} = \frac{Z_1}{Z_2}, \tag{1}$$

where $Z_i$ is the partition function for electronic state $i$. For parallel, shifted diabatic surfaces, we expect

$$\frac{P_1}{P_2} = e^{-\Delta E/kT}. \tag{2}$$

Here $\Delta E$ is the difference in energy between the electronic states, $k$ is Boltzmann's constant, and $T$ is temperature. Tully has shown that, unlike for surface hopping, Ehrenfest does not recover the exponential scaling in Eq. (2) even for a simple model with parallel, unshifted adiabatic surfaces.[37,38] More recently, Miller and Cotton have shown that, with windowing on top of mean-field dynamics, their SQC algorithm does recover detailed balance for the specific Hamiltonian in Refs. 37 and 38. In this paper, we will strenuously test Ehrenfest-like models (including SQC) for detailed balance using Hamiltonians (quadratic and anharmonic) where the diabatic states are not parallel and can be strongly displaced.

Our study below will be limited exclusively to the most inexpensive dynamics algorithms, i.e., those that do not require any phase cancellation for convergence of populations. In particular, we will consider the following three mean-field-dressed algorithms (with some additional options as well therein):

- Ehrenfest (mean-field) dynamics.[39]
- Meyer-Miller-Stock-Thoss (MMST)[23,24] dynamics (also known as the Poisson Bracket Mapping Equation (PBME)[11,12,27]).
- Symmetrical Quasi-Classical (SQC) dynamics[40] which follows MMST/PBME dynamics but windows the final trajectories.

For comparison with non-mean-field models, we will also compare against the following:

- Tully's Fewest Switches Surface Hopping (FSSH).[1,21]
- Our group's Augmented A-FSSH algorithm (which includes a decoherence correction).[41–43]

We will consider Coker's Partially Linearized Density Matrix[44] and Kapral's Forward-Backward Trajectory Solution[45] in a future publication.

For the current paper, we restrict ourselves to the case of two electronic states and we analyze three different, important regimes: harmonic systems with weak electronic coupling, harmonic systems with strong electronic coupling, and anharmonic systems with weak electronic coupling. Using exact solutions for the harmonic systems, as well as perturbation theory for the anharmonic systems, we will develop intuition for when these algorithms can be trusted and when they should fail.

## II. THEORETICAL METHODS

Before presenting our model Hamiltonians and results, we briefly review the relevant mixed quantum-classical methods (which are listed in Table I). Our purpose here is to use the same variable set to describe all of these algorithms, so as to make clear what the are the similarities and differences between them. Derivations of these methods, as well as practical recipes for propagating them, can be found in Refs. 1, 11, 23, 39, 40, and 42. In short, all of the algorithms in Table I propagate the same set of variables, but with differences as far as (i) the initial amplitude coefficients, (ii) the calculation of the final populations, and (iii) the PES used to defined the force, as we now discuss.

TABLE I. The different algorithms analyzed in this paper. The algorithms differ in their choices of initial conditions for the amplitudes, their approach to computing observables (binned or not binned), and their choice of PES for nuclear propagation. Note that the more common version of Miller's SQC algorithm[31] is referred to in this paper as SQCa. For PBME dynamics, in order to investigate the parameter $\gamma$ easily, we use the initial conditions from Eq. (8) (as opposed to the more standard prescription presented in the Appendix).

| Summary of relevant methods | | | | |
|---|---|---|---|---|
| Method | Acronym | Initial $c_i$ Eq. | Final $P_i$ Eq. | PES Eq. |
| Ehrenfest (mean-field) | MF | (7) | (9) | (16) |
| Binned Ehrenfest | MFb | (7) | (12) | (16) |
| Poisson Bracket Mapping Equation[11,23] | PBME | (8) | (9) | (18) |
| Poisson Bracket Mapping Equation with average surface | PBMEa | (8) | (9) | (20) |
| Symmetrical Quasi-Classical Windowing[40] | SQC | (8) | (12) | (18) |
| Symmetrical Quasi-Classical Windowing with average surface[31] | SQCa | (8) | (12) | (20) |
| Surface Hopping Standard[1] (w/o decoherence) | FSSH | (7) | (10) | (14) |
| Augmented with decoherence[42] | A-FSSH | | | |

### A. Similarities: Variable choice and equations of motion

We choose a Hamiltonian with two electronic states and a bath of $N_B$ classical degrees of freedom. For such a problem, all mixed quantum-classical algorithms discussed here propagate a set of $N_B$ position variables ($\vec{x}$), a set of $N_B$ momentum variables ($\vec{p}$), and a set of amplitudes $(c_1, c_2)$ for the wavefunction $|\Psi\rangle$, $|\Psi\rangle = c_1|\phi_1\rangle + c_2|\phi_2\rangle$. Here, we can imagine $\{|\phi_1\rangle, |\phi_2\rangle\}$ as a set of either diabatic or adiabatic states. The equations of motion are

$$\frac{dx_\sigma}{dt} = \frac{p_\sigma}{m_\sigma}, \tag{3}$$

$$\frac{dp_\sigma}{dt} = F_\sigma(\vec{x}). \tag{4}$$

Here $\sigma$ is an index for nuclear coordinates. The choice of $F_\sigma(\vec{x})$ will be defined below.

If we work in a diabatic basis, the amplitudes are propagated according to

$$\frac{dc_i}{dt} = -\frac{i}{\hbar}\sum_j H_{ij}^{di}(\vec{x})c_j. \tag{5}$$

Here $m_\sigma$ is the mass, and $H_{ij}^{di}(\vec{x})$ is the electronic Hamiltonian in a diabatic basis. The off-diagonal matrix element $H_{12}^{di}(\vec{x})$ is known as the electronic coupling which we assume to be independent of position, $H_{12}^{di}(\vec{x}) = H_{12}^{di}$, in the so-called "site" diabatic basis (i.e., the Condon approximation).

If we work in an adiabatic basis, the amplitudes are propagated according to

$$\frac{d\tilde{c}_i}{dt} = -\frac{i}{\hbar}H_{ii}^{ad}(\vec{x})\tilde{c}_i - \sum_j\sum_\sigma \frac{p_\sigma}{m_\sigma}d_{ij}^\sigma\tilde{c}_j. \tag{6}$$

Here, $d_{ij}^\sigma = \langle\phi_i|\frac{d}{dx_\sigma}|\phi_j\rangle$ is the derivative coupling between adiabatic states $|\phi_i\rangle$ and $|\phi_j\rangle$, and $H_{ij}^{ad}(\vec{x})$ is the electronic Hamiltonian in the adiabatic basis.

Let us now discuss the differences between the algorithms listed in Table I.

### B. Differences

Henceforward, equations will be written in a site-diabatic basis, unless otherwise noted.

#### 1. Initial coefficients

For simplicity, we will assume below that we initialize all dynamics (at time zero) with all population in one diabatic state. For the algorithms in Table I, there are different approaches towards choosing the initial coefficients of the amplitudes, $c_i$. For surface hopping and Ehrenfest dynamics, the initial conditions are normalized and chosen as

$$(c_1, c_2) = (1,0) \quad \text{or} \quad (0,1). \tag{7}$$

Additionally, for surface hopping, an integer $\lambda$ is assigned to each trajectory probabilistically to keep track of the active surface in the adiabatic basis.

For PBME and SQC, a different technique is invoked in order to include zero point energy (ZPE) effects. Now, the total norm of the amplitudes is larger than one and is, in practice, smeared out over a window to introduce uncertainty into the initial conditions. More precisely, for SQC dynamics, the initial coefficients are chosen as

$$c_i = \sqrt{N_i + 2\cdot RN\cdot\gamma}\; e^{i\theta}. \tag{8}$$

Here, $\theta$ is a random number chosen from a uniform distribution from $(0,1)$ multiplied by $2\pi$ and $N_i$ is 1 or 0 depending on whether diabatic state $i$ is initially occupied or unoccupied. $RN$ is a random number chosen from a uniform distribution from $[0,1]$. While each trajectory can carry its own norm, on average, the norm of the amplitudes is $1 + 2\gamma$.

Finally, the choice of initial conditions for true PBME dynamics is a bit more involved, but effectively the same: one chooses a norm for the amplitudes that exceeds unity. See the Appendix. For our purposes below, we will use either Eq. (7) or (8). For PBME, it is standard to choose $\gamma = 1/2$. See Ref. 34 for an interesting discussion on the nuances of initial amplitudes and how one can choose such initial conditions to optimize short-time dynamics in general.

#### 2. Final populations

Let $N^t$ be the total number of trajectories. We use $\alpha$ to index trajectories and $i, j, k$ and $l$ refer to electronic states. We define $n_{i\alpha} = |c_{i\alpha}|^2 - \gamma$ or $n_{i\alpha} = |c_{i\alpha}|^2$ depending on whether ZPE was included or not, respectively. There are then three different methods for calculating the final populations of each state.

The first method is to average over the populations of each trajectory according to their amplitudes

$$P_i = \frac{1}{N^t}\sum_{\alpha=1}^{N^t} n_{i\alpha} \quad i = 1,2. \tag{9}$$

Eq. (9) with $n_{i\alpha} = |c_{i\alpha}|^2$ is the Ehrenfest approach.

The second method for calculating populations (as relevant for surface hopping only) is to use a mixed quantum-classical density matrix.[46,47] This prescription takes into account both the trajectory's active surface as well as the amplitudes.

$$P_i = \frac{1}{N^t}\sum_{\alpha=1}^{N^t}\left(\sum_k |U_{ik}(\vec{x}^\alpha)|^2\delta_{k,\lambda^\alpha} + \sum_{k<j} 2\mathrm{Re}(U_{ik}(\vec{x}^\alpha)c_{k\alpha}c_{j\alpha}^* U_{ji}(\vec{x}^\alpha))\right). \tag{10}$$

Here, because surface hopping is run in an adiabatic basis, the matrix elements are transformed into a diabatic basis. $\mathbf{U}(\vec{x}^\alpha)$ is the local rotation matrix from the adiabatic basis to the final basis.

The third method for computing final populations is histogramming each trajectory based on the amplitudes. Such binning has been recommended by Miller and Cotton to correct Ehrenfest populations.[40] While different variations

have been recommended,[32] henceforward we will use the Cotton-Miller windowing function[10]

$$W_N(n) = \frac{1}{\Delta n} H\left(\frac{\Delta n}{2} - |n - N|\right) \tag{11}$$

based on a Heaviside function, $H(z) = \begin{cases} 0, & z < 0, \\ 1, & z > 0, \end{cases}$. Here $\Delta n$ is the window width and $N$ is 0 or 1. The final population for state $i$ is then,

$$P_i = \frac{\sum_{\alpha=1}^{N^t} W_1(n_{i\alpha}) \cdot \prod_{j\neq i} W_0(n_{j\alpha})}{\sum_{\alpha=1}^{N^t} \sum_k W_1(n_{k\alpha}) \cdot \prod_{l\neq k} W_0(n_{l\alpha})}. \tag{12}$$

For SQC, the window width is chosen to be $\Delta n = 2\gamma$, which symmetrically windows the initial conditions (through Eq. (8)) and the final conditions (through Eq. (12)). Cotton and Miller suggest $\gamma = 0.366$ as the optimal choice of $\gamma$.[10,31] Below, whenever such windows are used, we will speak interchangeably of "windowing" or "binning" dynamics.

### 3. Potential energy surface

Between surface hopping and mean-field approaches, the biggest difference is how to deal with multiple PESs and establish the relevant force $F_\sigma(\vec{x})$ for dynamics in Eq. (4). In a fixed diabatic basis (the "site" basis) with Hamiltonian $H_{ij}(\vec{x})$, we define the force from the $i$th diabatic electronic state to be:

$$F^i_\sigma(\vec{x}) \equiv -\frac{dH_{ii}}{dx_\sigma}. \tag{13}$$

For surface hopping, the relevant PES is a single adiabatic state, which is known as the active surface. The trajectory stochastically hops between different surfaces. For a two state Hamiltonian, these adiabatic states are

$$V(\vec{x}) = \frac{H_{11}(\vec{x}) + H_{22}(\vec{x})}{2} \pm \frac{1}{2}\sqrt{(H_{11}(\vec{x}) - H_{22}(\vec{x}))^2 + 4H_{12}^2}, \tag{14}$$

with forces

$$F_\sigma(\vec{x}) = \frac{1}{2}\left(F^1_\sigma(\vec{x}) + F^2_\sigma(\vec{x})\right) \pm \frac{1}{2}\frac{(H_{11}(\vec{x}) - H_{22}(\vec{x}))}{\sqrt{(H_{11}(\vec{x}) - H_{22}(\vec{x}))^2 + 4H_{12}^2}} \times \left(F^1_\sigma(\vec{x}) - F^2_\sigma(\vec{x})\right). \tag{15}$$

For Ehrenfest dynamics (i.e., the simplest form of mean-field dynamics), one uses the dynamical expectation value of the electronic Hamiltonian as the PES. For a two state Hamiltonian, this dynamic PES and the corresponding force are

$$V(\vec{x}) = |c_1|^2 H_{11}(\vec{x}) + |c_2|^2 H_{22}(\vec{x}) + H_{12}(c_1^* c_2 + c_1 c_2^*), \tag{16}$$

$$F_\sigma(\vec{x}) = |c_1|^2 F^1_\sigma(\vec{x}) + |c_2|^2 F^2_\sigma(\vec{x}). \tag{17}$$

Mean-field forces are complicated slightly by the inclusion of ZPE in the wavefunction, because the relevant amplitudes are no longer normalized (as in Eq. (8)). For PBME and SQC like approaches, one must remove the electronic ZPE from the populations (i.e., subtract $\gamma$ from each of the $|c_i|^2$'s) before computing the potential energy. For a two state Hamiltonian, this subtraction leads to the following PES and force

$$V(\vec{x}) = (|c_1|^2 - \gamma)H_{11}(\vec{x}) + (|c_2|^2 - \gamma)H_{22}(\vec{x}) + H_{12}(c_1^* c_2 + c_1 c_2^*), \tag{18}$$

$$F_\sigma(\vec{x}) = (|c_1|^2 - \gamma)F^1_\sigma(\vec{x}) + (|c_2|^2 - \gamma)F^2_\sigma(\vec{x}). \tag{19}$$

Finally, as pointed out by Kelly *et al.*[28] and Miller *et al.*,[10,31] it is helpful to decompose the Hamiltonian into the sum of an average surface plus the expectation value of a shifted electronic Hamiltonian. For a two state Hamiltonian, this premise leads to

$$V(\vec{x}) = \frac{1}{2}(H_{11}(\vec{x}) + H_{22}(\vec{x})) + \frac{1}{2}(|c_1|^2 - |c_2|^2)(H_{11}(\vec{x}) - H_{22}(\vec{x})) + H_{12}(c_1^* c_2 + c_1 c_2^*) \tag{20}$$

$$F_\sigma(x) = \frac{1}{2}\left(F^1_\sigma(\vec{x}) + F^2_\sigma(\vec{x})\right) + \frac{1}{2}(|c_1|^2 - |c_2|^2)\left(F^1_\sigma(\vec{x}) - F^2_\sigma(\vec{x})\right). \tag{21}$$

On one hand, if we consider Ehrenfest trajectories, where $|c_1|^2 + |c_2|^2 = 1$, then Eq. (20) is equivalent to Eq. (16). On the other hand, for any set of trajectories for which $|c_1|^2 + |c_2|^2 = 1 + 2\gamma$, Eq. (20) is equivalent to Eq. (18). However, for PBME and SQC dynamics using smeared initial conditions (i.e., Eq. (8) for the initial coefficients), Eq. (20) is not equivalent to Eq. (18). We will show below how using Eq. (20) differs from Eq. (18). See also Ref. 28.

For reference, Table I summarizes all of the algorithms we consider below, highlighting the relevant equations and the acronyms we use for shorthand.

## III. RESULTS

### A. Spin-boson Hamiltonian

We begin our study with the famous spin-boson Hamiltonian, and we consider the cases of both weak and strong electronic coupling, $V_c$. The spin-boson Hamiltonian couples a two-level electronic system to a bath of harmonic oscillators with positions ($\vec{x}$) and momenta ($\vec{p}$). It can be written as

$$H_{Spin\text{-}Boson}(\vec{x},\vec{p}) = H_s + H_{sb}(\vec{x}) + H_b(\vec{x},\vec{p}), \tag{22}$$

$$H_s = \begin{bmatrix} 0 & V_c \\ V_c & -\epsilon_0 \end{bmatrix}, \tag{23}$$

$$H_{sb}(\vec{x}) = \sum_\sigma \begin{bmatrix} d_\sigma x_\sigma & 0 \\ 0 & -d_\sigma x_\sigma \end{bmatrix}, \tag{24}$$

$$H_b(\vec{x},\vec{p}) = \sum_\sigma \frac{p_\sigma^2}{2m_\sigma} + \frac{1}{2}m_\sigma\omega_\sigma^2 x_\sigma^2 + \frac{d_\sigma^2}{2m_\sigma\omega_\sigma^2}. \tag{25}$$

Here $H_s$ is the system Hamiltonian, $H_{sb}$ is the system-bath coupling and $H_b$ is the bath Hamiltonian. The driving force between the electronic states is $\epsilon_0$. The frequency of bath mode $\sigma$ is $\omega_\sigma$ and the coupling strength of mode $\sigma$ is $d_\sigma$, which defines the spectral density,

$$J(\omega) = \frac{\pi}{2}\sum_\sigma \frac{d_\sigma^2}{m_\sigma \omega_\sigma}\delta(\omega - \omega_\sigma). \tag{26}$$

One overall measure of the coupling of the electronic system to the bath is the reorganization energy,

$$E_r = \frac{4}{\pi}\int_0^\infty d\omega \frac{J(\omega)}{\omega}. \tag{27}$$

Below, for the most part, we will use the Brownian spectral density,

$$J_{Brown}(\omega') \equiv \frac{1}{2}E_r \frac{\omega^2 \eta \omega'}{(\omega'^2 - \omega^2)^2 + \eta^2 \omega'^2}. \tag{28}$$

Whereas many oscillator modes are coupled to the two-level electronic system in Eq. (24), for the unique case of the Brownian spectral density in Eq. (28), the spin-boson Hamiltonian can be transformed through a change of basis into a different form whereby only a single, primary bath mode is coupled directly to the two-level system. However, that single bath mode (with position $x$ and momentum $p$) is now coupled to an auxiliary nuclear bath (with positions $\vec{Q}$ and momenta $\vec{P}$) whose net effect is to damp the motion of the primary bath mode while introducing a random force (i.e., the primary mode will experience Langevin dynamics[48]).

Mathematically, after a change in basis, the Hamiltonian can be written as

$$H_{Spin\text{-}Boson}(x,p,\vec{Q},\vec{P}) = \frac{p^2}{2m} + H_0(x) + H_I(x,\vec{Q}) + H_B(\vec{Q},\vec{P}) + H_{Ren}(x), \tag{29}$$

$$H_0(x) = \begin{bmatrix} \frac{1}{2}m\omega^2 x^2 & V_c \\ V_c & \frac{1}{2}m\omega^2(x-\lambda)^2 - \epsilon_0 \end{bmatrix}, \tag{30}$$

$$H_I(x,\vec{Q}) = \sum_\sigma \zeta_\sigma Q_\sigma x, \tag{31}$$

$$H_B(\vec{Q},\vec{P}) = \sum_\sigma \frac{P_\sigma^2}{2m_\sigma} + \frac{1}{2}m_\sigma \omega_\sigma^2 Q_\sigma^2, \tag{32}$$

$$H_{Ren}(x) = \sum_\sigma \frac{\zeta_\sigma^2 x^2}{2m_\sigma \omega_\sigma^2}. \tag{33}$$

Here $H_0(x)$ is the quantum subsystem coupled to the primary mode, $\lambda$ is the horizontal shift of the primary bath mode, and the reorganization energy is $E_r \equiv m\omega^2\lambda^2/2$. $H_B(\vec{Q},\vec{P})$ is the Hamiltonian for the auxiliary bath coupled to the primary mode by $H_I(x,\vec{Q})$ (and renormalized by $H_{Ren}(x)$). The coupling between the primary mode and auxiliary bath can be shown to be purely Ohmic with spectral density

$$J_{Ohmic}(\omega) = \frac{\pi}{2}\sum_\sigma \frac{\zeta_\sigma^2}{m_\sigma \omega_\sigma}\delta(\omega - \omega_\sigma) = m\eta\omega. \tag{34}$$

The purely Ohmic form of Eq. (34) allows us to integrate out the nuclear bath modes and simulate dynamical friction with Langevin equation.[49,50] In practice, if $F(x)$ is the gradient used by a semiclassical method to describe a system with Hamiltonian $H_0(x)$ in Eq. (30), the relevant form is now:

$$F_{tot}(x) = F(x) - \eta p + \xi. \tag{35}$$

Here, $\xi$ is the random force term sampled from a Gaussian distribution with standard deviation $\sqrt{2\eta m k_B T/dt}$ and $\eta$ is the frictional damping.

Below, we will simulate dynamics sometimes with a full bath of nuclei and sometimes with a Langevin force. Whenever we simulate classical dynamics, we set the mass equal to 1.

### 1. Weak electronic coupling: Populations

In Figure 1, we plot the ratio of equilibrium populations in the site basis as a function of driving force ($\epsilon_0$). The dynamics of several such methods in Table I have already been analyzed[10,31] (in the site basis) in this weak electronic coupling regime. We include all relevant methods for a complete comparison. Our choice of parameter is: $kT = 5, V_c = 0.2kT, \hbar\omega = 0.6kT$, and $E_r = 3.6kT$. The friction, $\eta$, is $\omega$. We consider several values of the windowing/ZPE parameter $\gamma$ in Eq. (8).

According to Figure 1, the surface hopping and SQCa approaches perform best at recovering detailed balance (i.e., Boltzmann statistics, Eq. (2)). Note that the SQCa results appear rather independent of the value of $\gamma$, though smaller values of $\gamma$ tend to work best. For all of the dynamical schemes (excluding surface hopping), we provide data showing populations with and without windowing the final trajectories. Note that windowing enhances all mean-field solutions; even straightforward Ehrenfest dynamics—which are known to give incorrect equilibrium populations[37,38]—recover the correct Boltzmann statistics with a small enough window.

A few words are now appropriate regarding surface hopping. We expect[37,38] surface hopping to nearly recover the correct equilibrium density matrix because, in the adiabatic basis, the trajectories are expected to sample the surfaces with the Boltzmann probability ($\exp(-\beta E(\vec{x}))$) due to frustrated hops (i.e., hops that are not allowed by energy conservation). Moreover, we can likely assume that, at equilibrium, the phases of the FSSH amplitudes at any time are essentially random, so that the coherence in the adiabatic basis averages to zero effectively. Thus, using the definition of the FSSH mixed quantum-classical density matrix in a locally adiabatic basis ($\rho^{eq}$) from Ref. 47, we expect

$$\rho^{eq}(\vec{x},\vec{p}) \approx \frac{\begin{bmatrix} e^{-\beta\left(\frac{\vec{p}^2}{2m} + H_{11}^{ad}(\vec{x})\right)} & 0 \\ 0 & e^{-\beta\left(\frac{\vec{p}^2}{2m} + H_{22}^{ad}(\vec{x})\right)} \end{bmatrix}}{\int d\vec{p}\int d\vec{x}\, e^{-\beta\left(\frac{\vec{p}^2}{2m} + H_{11}^{ad}(\vec{x})\right)} + e^{-\beta\left(\frac{\vec{p}^2}{2m} + H_{22}^{ad}(\vec{x})\right)}}. \tag{36}$$

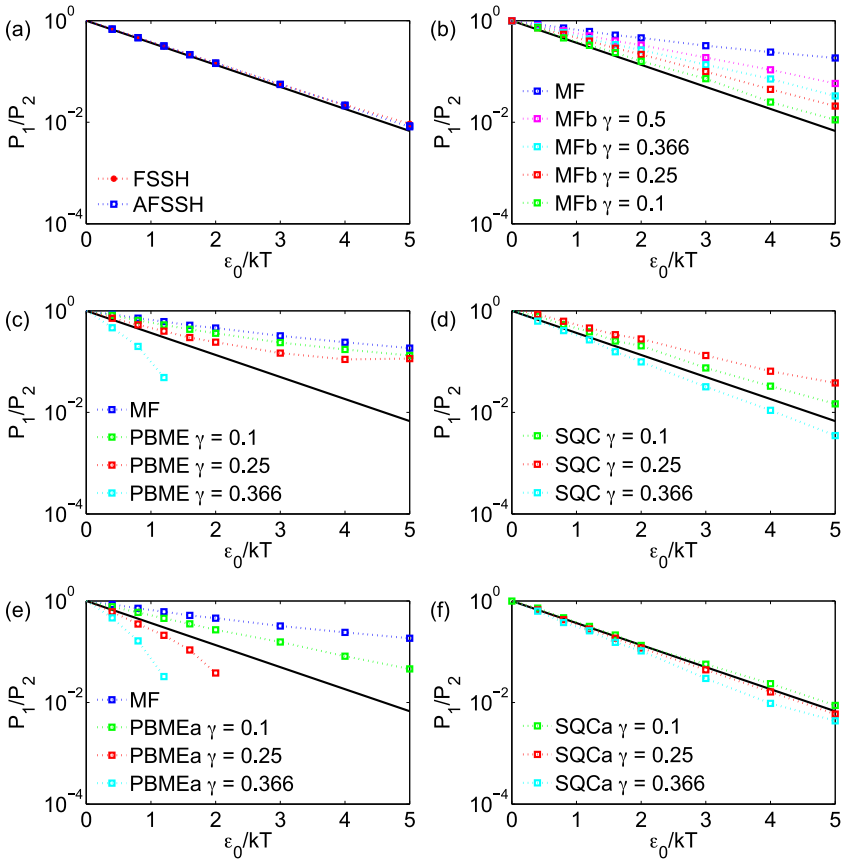


FIG. 1. The equilibrium population ratio for the spin-boson Hamiltonian as a function of the driving force, $\epsilon_0$, for a variety of $\gamma$ values (see Eq. (8)).[51] $kT = 5, V_c = 0.2kT, \hbar\omega = 0.6kT, E_r = 3.6kT, \eta = \omega$. Note that we are operating in the limit of small diabatic coupling in the site basis. The solid black line in each plot is the correct Boltzmann solution (Eq. (2)). Each plot shows various approaches, including (a) surface hopping methods, (b) simple Ehrenfest, and subsequent windowing, (c) PBME, (d) SQC, (e) PBMEa, and (f) SQCa. See Table I for a list of acronyms. Note that surface hopping and mean-field results with small windows (especially SQCa) nearly recover detailed balance for their equilibrium populations. Not all data points for PBME can be included in this semilog plot, as this method sometimes has negative average population ratios. All mixed quantum-classical data are calculated with classical Langevin dynamics.

Of course, $\rho^{eq}$ can always be transformed from the locally adiabatic representation into any other basis. Equation (36) is consistent with Boltzmann statistics in the weak coupling limit.

### 2. Weak electronic coupling: Coherences

Within the weak electronic coupling regime, we also consider the effect of a change of basis. In Figure 2, we plot the ratio of equilibrium populations as a function of driving force $\epsilon_0$ in a so-called "half–half" basis (which is calculated by transforming from the site basis with matrix $\mathbf{U}_{half}$)

$$|\Psi_{half}\rangle = \mathbf{U}_{half}|\Psi\rangle, \tag{37}$$

$$\mathbf{U}_{half} = \sqrt{\frac{1}{2}}\begin{bmatrix} 1 & 1 \\ 1 & -1 \end{bmatrix}. \tag{38}$$

For these calculations, we can estimate the correct answer by preforming exact diagonalization and then invoking the fact that the electronic coupling is perturbatively small. In other words, we construct the equilibrium reduced density matrix by first constructing our Hamiltonian in the basis of harmonic oscillator modes and bosonic states, and we then calculate $\exp(-\beta H)$ and trace out the bath. To converge, we used 40 harmonic oscillator modes.

According to Figure 2, FSSH recovers the correct population ratio as compared against exact diagonalization. By contrast, Ehrenfest does not recover the correct populations and windowing does not help. Calculations that include ZPE do a better job of getting the correct result in this basis, though not always much better. Interestingly, SQC with $\gamma = 0.366$ (the value recommended by Miller[31]) does quite well in this case.[52] For this reason, below we will focus on the SQC $\gamma = 0.366$ algorithm as a point of comparison. Finally, for all mean-field dynamical algorithms (i.e., everything except surface hopping), narrowing the windows makes the results worse.

### 3. Strong electronic coupling

We now turn to the regime of strong electronic coupling, where we investigate both site and excitonic bases. Our choice of parameters is $kT = 5, \hbar\omega = 0.5kT, E_r = 0.25kT, \epsilon_0 = 2kT$ and $\eta = 10\omega$. By choosing $E_r$ to be very small, we can estimate the exact populations by computing $\rho = \exp(-\beta H_s)/\mathrm{Tr}[\exp(-\beta H_s)]$ (see Eq. (23)), where we ignore small system-bath coupling.

In Figure 3, we plot equilibrium population ratios in the site basis as a function of $V_c$. We plot FSSH and SQCa populations. We consider several different versions of the SQCa algorithm. Most simply, we can simulate a classical bath, either with (i) a large number of oscillator modes or (ii) with a single mode that experiences a Langevin force. These results are (of course) identical. Going beyond classical distributions, one can also simulate a quantum bath with a quasi-classical distribution function of velocities (to include zero point energy for high frequency oscillators). See discussion.

SQCa with a classical bath does not recover the correct long time limits, but SQCa does recover the correct long-time

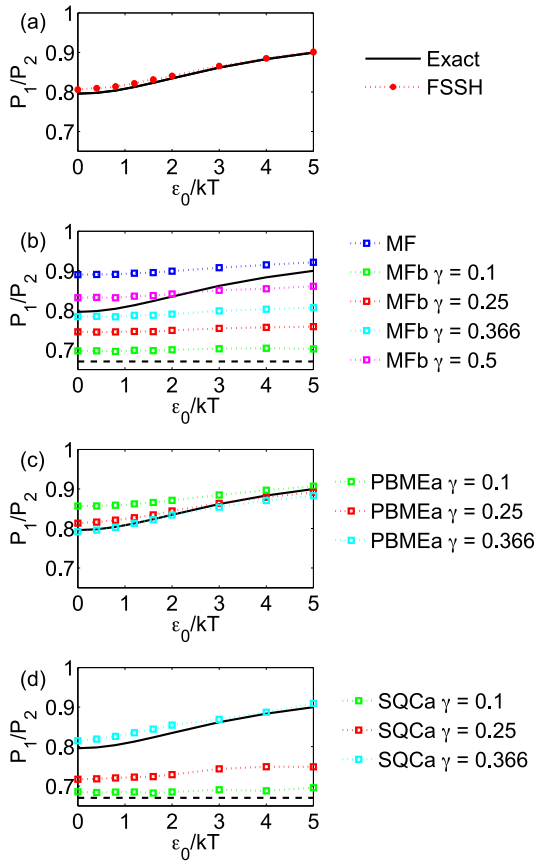


FIG. 2. The equilibrium ratio of populations of the electronic states in the half-half basis as a function of $\epsilon_0$, the driving force, for a variety of $\gamma$ values.[51] $kT = 5, V_c = 0.2kT, \hbar\omega = 0.6kT, E_r = 3.6kT, \hbar\eta = 5kT$. Note that these data come from the regime with weak diabatic coupling in the site basis. Each plot shows various approaches, including (a) FSSH, (b) simple Ehrenfest and subsequent binning, (c) PBMEa, and (d) SQCa. The black line shows exact results. Only FSSH, PBMEa, and SQCa with $\gamma = 0.366$ retain the correct ratio of equilibrium populations in this new basis. The black dashed line in panels (b) and (d) is the value $\exp(-2\beta V_c) = \exp(-2/5) = 0.67$; see Section IV. See text for a discussion of how the exact populations were calculated. All mixed quantum-classical data calculated with classical Langevin dynamics.

limits with a quantum bath. Surface hopping also closely follows the correct equilibrium trend.

Next, we consider a change of basis for these same systems. To construct the so-called "excitonic basis," the electronic Hamiltonian, $H_0(x)$, is diagonalized at position $x = \lambda/2$, leading to eigenvectors $\mathbf{U}_{Excitonic}$ (recall that $\lambda = \sqrt{2E_r/m\omega^2}$). The transformation from site to excitonic basis is then:

$$|\Psi_{Excitonic}\rangle = \mathbf{U}_{Excitonic}|\Psi\rangle \tag{39}$$

$$\mathbf{U}_{Excitonic} = \sqrt{\frac{1}{2}}\begin{bmatrix} \sqrt{1+\frac{\epsilon_0/2}{\sqrt{(\epsilon_0/2)^2+V^2}}} & \sqrt{1-\frac{\epsilon_0/2}{\sqrt{(\epsilon_0/2)^2+V^2}}} \\ \sqrt{1-\frac{\epsilon_0/2}{\sqrt{(\epsilon_0/2)^2+V^2}}} & -\sqrt{1+\frac{\epsilon_0/2}{\sqrt{(\epsilon_0/2)^2+V^2}}} \end{bmatrix}. \tag{40}$$

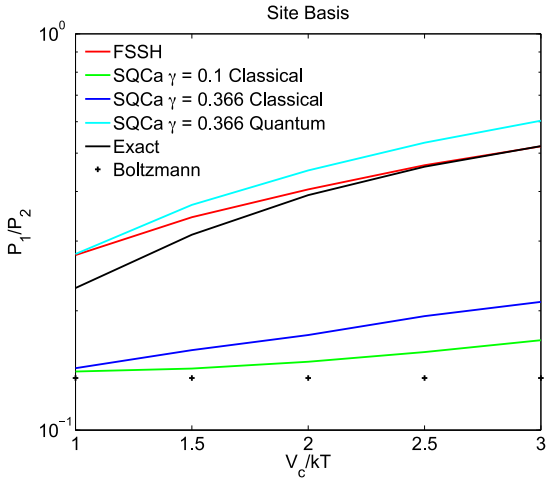


FIG. 3. The equilibrium ratio of populations of the electronic states in the site basis as a function of $V_c$, the electronic coupling, with $kT = 5, \hbar\omega = 0.5kT, E_r = 0.25kT, \epsilon_0 = 2kT, \eta = 10\omega$. The black line marks the exact solutions (see text) whereas the black dots note the Boltzmann ratio in the site basis ($\exp(-\beta\epsilon_0) = \exp(-2) = 0.14$). On the one hand, both classical FSSH and SQCa with a quantum bath follow the correct trend. On the other hand, SQCa with a classical bath does not follow the correct trend; instead the SQCa population is closer to the Boltzmann ratio (which is incorrect in the site basis). See Section IV for analysis of quantum bath conditions.

Figure 4 plots population ratios in this excitonic basis. For these systems, the equilibrium population of the upper diabat will be infinitesimal at equilibrium. That being said, observe that the SQCa method with a classical bath performs best at recovering the long time limits. By contrast, FSSH slightly overestimates the long time population but follows the correct trend. The populations from SQCa with a quantum bath do not follow the correct trend.

These results will be discussed in Section IV.

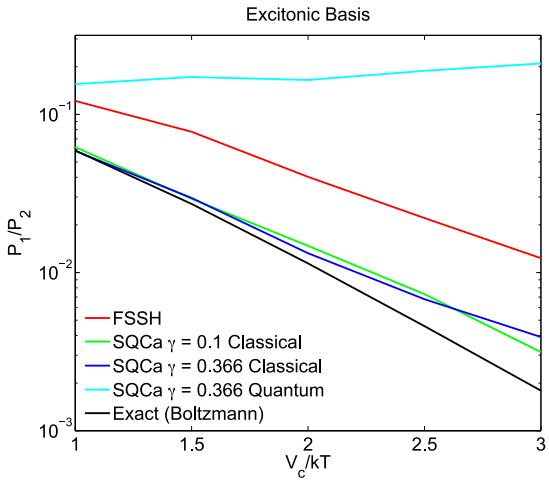


FIG. 4. The equilibrium ratio of populations of the electronic states in the excitonic basis as a function of $V_c$, the electronic coupling, with $kT = 5, \hbar\omega = 0.5kT, E_r = 0.25kT, \epsilon_0 = 2kT, \eta = 10\omega$. The black line denotes the exact solution, which is equivalent to the Boltzmann ratio between the exciton states (which are weakly coupled). Both FSSH and SQCa with a classical bath follow the correct trend, while SQCa with a quantum bath behaves erroneously. See Section IV for analysis of quantum bath conditions.

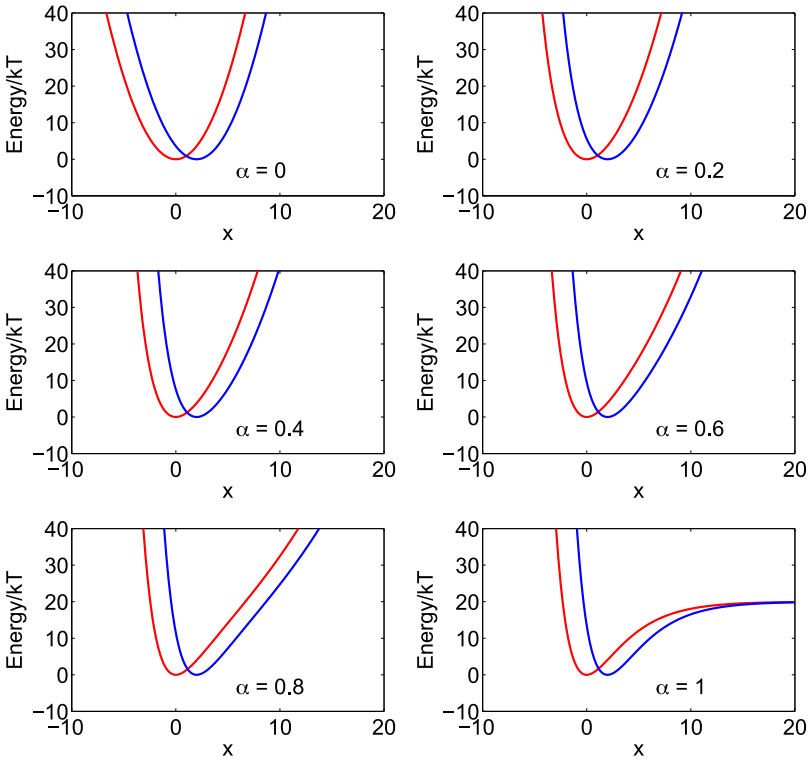


FIG. 5. The potential energy surfaces of the two electronic states as a function of $\alpha$, the Morse character in Eq. (41). When $\alpha = 0$, the system is simply the symmetric spin-boson Hamiltonian. When $\alpha = 1$, the states are two weakly coupled Morse oscillators with the same energy minima.[29]

### B. Anharmonicity

At this point, we have presented data from a few spin-boson Hamiltonians. We have seen that, by including ZPE for initial conditions and windowing the final trajectories, the SQCa approach can recover many of the correct features of detailed balance—though curiosities arise when we consider classical versus quantum baths for the case of strong off-diagonal coupling between diabats.

To go beyond these harmonic models and study anharmonicity, we now consider a new Hamiltonian where we slowly change the harmonic wells of the spin-boson Hamiltonian into a set of coupled Morse oscillators.[29] We parameterize the system Hamiltonian by a variable $\alpha$,

$$H_s(x) = \frac{p^2}{2m} + (1-\alpha)H_{Harmonic}(x) + \alpha H_{Morse}(x), \tag{41}$$

$$H_{Harmonic}(x) = \begin{bmatrix} \frac{1}{2}m\omega^2 x^2 & V_c \\ V_c & \frac{1}{2}m\omega^2(x-\lambda)^2 - \epsilon_0 \end{bmatrix}, \tag{42}$$

$$H_{Morse}(x) = \begin{bmatrix} D_e(1-e^{-ax})^2 & V_c \\ V_c & D_e(1-e^{-a(x-\lambda)})^2 - \epsilon_0 \end{bmatrix}, \tag{43}$$

where $D_e = 20kT$, $a = 0.3$, $\lambda = 2$, $V_c = 0.2kT$, $m = 1$, $\hbar\omega = 0.6kT$, and $kT = 5$. As for the spin-boson model, the system Hamiltonian is linearly coupled to an auxiliary bath to introduce friction and open boundary conditions. For simplicity, we consider only Langevin dynamics, which (as stated above) implies a classical bath of auxiliary modes. We set the driving force $\epsilon_0 = 0$ and damping parameter $\eta = 3$. In this case, because $V_c$ is small, at equilibrium the population on each surface is expected to be 0.5, independent of $\alpha$. The $H_{11}(x)$ and $H_{22}(x)$ surfaces are depicted in Figure 5.

As we scan over $\alpha$ in Figure 6, no mean-field approach recovers the correct equilibrium populations for systems with anharmonicity. For the windows plotted, Ehrenfest and all windows thereof underestimate $P_1$ while all other approaches and their windows over estimate $P_1$. From the data, it seems likely that, with a small enough value of $\gamma$ for the windowing, any and all of the mean-field approaches can recover detailed balance ($P_1 = P_2$). Note that surface hopping approaches always recover detailed balance.

## IV. DISCUSSION

We have presented above a reasonably large set of data. Overall, for harmonic systems, adding zero point energy plus windowing on top of Ehrenfest dynamics almost always helps; at times, ZPE corrected mean-field theories with windowing do outperform surface hopping for some populations. However, two observations above must now be explained: (i) For the spin-boson model with strong electronic coupling, we find that choice of initial bath conditions can greatly effect the final answer in a basis dependent fashion. (ii) For anharmonic systems, surface hopping is always the most reliable and the SQCa model falters. Let us now interpret and digest all of the relevant information.

### A. The choice of windowing parameter versus choice of basis

From Figures 1 and 6, it is empirically clear that, in the regime of weak electronic coupling, a small window ($\gamma$) yields the best equilibrium populations, in close agreement with Boltzmann statistics. This achievement can be rationalized if

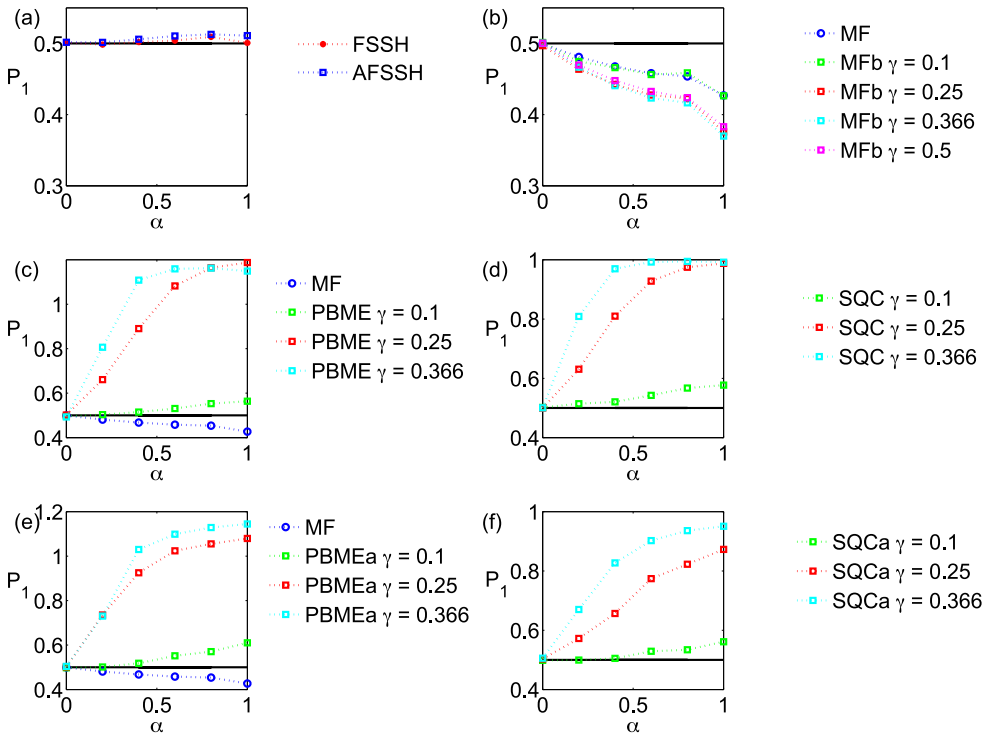


FIG. 6. The equilibrium population for electronic state 1 ($P_1$) as a function of the Morse character, $\alpha$, for the Hamiltonian in Eq. (41) with $D_e = 20kT$, $a = 0.3, \lambda = 2, V_c = 0.2kT, \hbar\omega = 0.6kT, \eta = \omega, m = 1$, and $kT = 5$. In this weak coupling limit, the correct answer is $P_1 = 0.5$ (black line). Each plot shows various approaches, including (a) surface hopping methods, (b) simple Ehrenfest and subsequent windowing, (c) PBME, (d) SQC, (e) PBMEa, and (f) SQCa. Note the different scales of the y-axis for each plot; where $P_1 > 0$, one finds negative populations.[53] Note also that, to recover detailed balance, one must use either surface hopping or a small window on top of mean-field theory ($\gamma \to 0$). All mixed quantum-classical data calculated with classical Langevin dynamics.

we take the limit that the window acts as a delta function on the populations. In such a case, if we convert the potential in Eq. (16) to action-angle variables, $n_i$ and $q_i$[24] using $c_i = \sqrt{n_i + \gamma}e^{-iq_i}$, the Hamiltonian becomes[23]

$$H = P^2/2M + V_{AA}(x) \tag{44}$$

$$V_{AA}(x, n_1, n_2, q_1, q_2) = n_1 H_{11}(x) + n_2 H_{22}(x) + 2V_c\sqrt{(n_1+\gamma)(n_2+\gamma)}\cos(q_1 - q_2). \tag{45}$$

At equilibrium, the ratio of populations at equilibrium can be calculated from the partition functions as

$$\frac{P_1}{P_2} = \frac{\int_{-\infty}^{\infty} dx \int_{1-2\gamma}^{1+2\gamma} dw Z_w^{-1} \int dn_1^f \int dn_2^f \int dq_1^f \int dq_2^f e^{-\beta H(x, n_1^f, n_2^f, q_1^f, q_2^f)} \delta(1 - n_1^f)\delta(n_2^f)}{\int_{-\infty}^{\infty} dx \int_{1-2\gamma}^{1+2\gamma} dw Z_w^{-1} \int dn_1^f \int dn_2^f \int dq_1^f \int dq_2^f e^{-\beta H(x, n_1^f, n_2^f, q_1^f, q_2^f)} \delta(n_1^f)\delta(1 - n_2^f)} \tag{46}$$

$$= \frac{\int_{-\infty}^{\infty} dx \int_{1-2\gamma}^{1+2\gamma} dw Z_w^{-1} \int dq_1^f \int dq_2^f e^{-\beta H(x, 1, 0, q_1^f, q_2^f)}}{\int_{-\infty}^{\infty} dx \int_{1-2\gamma}^{1+2\gamma} dw Z_w^{-1} \int dq_1^f \int dq_2^f e^{-\beta H(x, 0, 1, q_1^f, q_2^f)}}. \tag{47}$$

We integrate over the initial distribution of actions, $w = n_1^i + n_2^i$, as well as over the final ($f$) values of the action-angle variables. The partition function $Z_w$ normalizes all probabilities. In the limit of very small $\gamma$ such that $(n_1, n_2) = (1, 0)$ or $(0, 1)$, the only contribution from the initial distribution will be from $w = 1$,

$$\frac{P_1}{P_2} = \frac{\int_{-\infty}^{\infty} dx e^{-\beta H_{11}(x)} \Delta w \int dq_1^f \int dq_2^f e^{-\beta 2V_c\sqrt{\gamma+\gamma^2}\cos(q_1^f - q_2^f)}}{\int_{-\infty}^{\infty} dx e^{-\beta H_{22}(x)} \Delta w \int dq_1^f \int dq_2^f e^{-\beta 2V_c\sqrt{\gamma+\gamma^2}\cos(q_1^f - q_2^f)}} \tag{48}$$

$$= \frac{\int_{-\infty}^{\infty} dx e^{-\beta H_{11}(x)}}{\int_{-\infty}^{\infty} dx e^{-\beta H_{22}(x)}}. \tag{49}$$

Eq. (49) makes clear that, for small windows, one must recover a Boltzmann ratio, i.e., the ratio of partition functions.[54] Note that Stock and co-workers have long argued that decreasing the amount of zero-point energy (i.e., changing $\gamma$) can be an effective means to achieve the correct long time populations.[35,36]

At this point, however, it is very important to note that Boltzmann ratios in Eqs. (2) and (49) are correct only when the electronic coupling is small and the diabatic states are minimally coupled. Thus, one must expect that windowing will fail when diabatic states are strongly coupled. This explains the failure of classical SQCa in Figure 3.

To further address this hypothesis, consider the data in Figure 2. In the half-half basis, the difference between the on-diagonal states is $2V_c$, independent of $\epsilon_0$ and $x$. Recall that the accuracy of the mean-field results decreases after windowing. As the window width gets smaller, the ratio approaches the hypothetical Boltzmann factor for the diagonal diabatic states, $e^{-\Delta E/kT} = e^{-2V_c/kT} = 0.67$.

Finally, we make one last observation. Note that, according to Figure 2, for the special case of $\gamma = 0.366$, SQCa dynamics do recover the correct populations in the half-half basis. For the moment, we are unsure of the source of this unexpected success of SQCa dynamics with the 0.366 parameter (independent of basis). This success might be very interesting to study in the future.

For now, we conclude that, if windowing is to be a universally reliable technique on top of classical mean-field theories, it would seem most natural to work in a weakly coupled basis (with small $\gamma$).

### B. Quantum vs. classical bath

The argument above explains why classical SQCa does not perform well in the site basis for long time populations, but it does perform extremely well in the excitonic basis. From Figure 3, however, one question remains: why does including a quantum bath perform so much better in the site basis (and less well in the excitonic basis)? One can fashion two possible explanations.

On one hand, perhaps quantum SQCa outperforms classical SQCa by sampling over the correct initial distribution functions that capture wavepacket widths and thereby introducing some quantum mechanical, non-classical dynamics?

On the other hand, there is a second possible explanation based on how one initializes a quasi-classical quantum bath. Whereas classical baths are initialized so that, on average, all bath modes have $\frac{1}{2}kT$ kinetic energy, quantum baths are initialized by sampling velocity from the Wigner distribution. As such, quantum baths include ZPE effects. In other words, the relevant momentum distributions have Gaussian widths $\sigma_{p\sigma} = \sqrt{m_\sigma/\beta}$ (for classical baths) instead of $\sigma_{p\sigma} = \sqrt{m_\sigma\omega_\sigma/2\tanh(\beta\omega_\sigma)}$ (for quantum baths). Now, in general, because each mode has its own zero point energy and we are simulating classical dynamics, we expect that kinetic energy will "leak" from high frequency modes into low frequency modes such that, at long times, all modes have the same kinetic energy.[55–59] Thus, perhaps quantum SQCa performs well because the modes equilibrate to a higher temperature through zero point leakage?

To distinguish between these explanations, Figure 7 shows the dynamics of SQCa and Ehrenfest with both classical and quantum bath distributions compared to exact data from

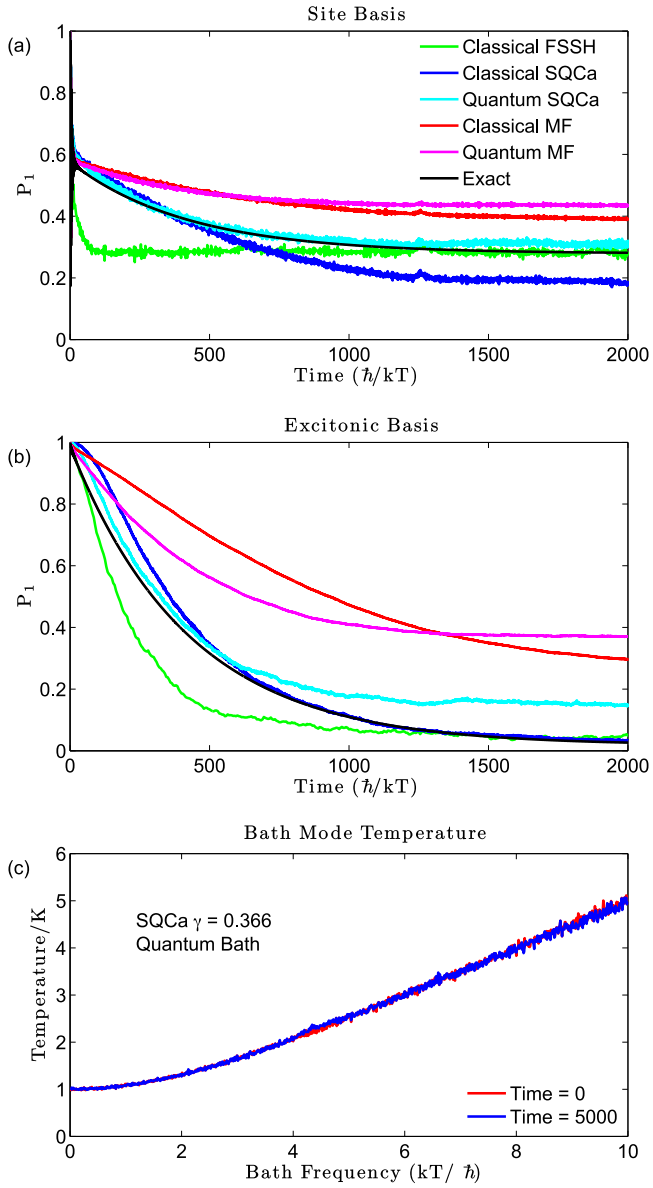


FIG. 7. Population dynamics in the (a) site and (b) excitonic basis for a Hamiltonian with a Drude spectral density (Eq. (50)) and parameters $kT = 5$, $V_c = 2kT, \hbar\omega = 0.5kT, E_r = 0.25kT, \epsilon_0 = 2kT, \eta = 10\omega$ (designed to mimic the Hamiltonian in Figs. 3 and 4). Here we compare Ehrenfest and FSSH dynamics against SQCa dynamics ($\gamma = 0.366$) with a quantum versus classical bath. The black lines are the exact dynamics from HEOM. On the one hand, in the site basis, SQCa with $\gamma = 0.366$ and a quantum bath recovers the correct dynamics. On the other hand, in the excitonic basis, the dynamics are better simulated with a classical bath. Regarding FSSH, surface hopping consistently recovers the correct equilibrium populations with a classical bath, but the short-time dynamics fail in the site diabatic basis.[65] This failure arises because the algorithm cannot accurately capture transient dynamics for long-lived coherences between wavepackets on different adiabatic surfaces; this is one example of the recoherence problem in FSSH.[42] (c) The temperature of each of the SQCa bath modes for the quantum bath at time 0 and 5000. The quantum bath does not relax to the classical limit, instead retaining the zero point energy in each mode.

HEOM[60–64] using the Hamiltonian from Figures 3 and 4 with $V_c = 2kT$. For this figure, we do not use a quantum Brownian oscillator spectral density (Eq. (28)), but rather a Drude spectral density

$$J_{Drude}(\omega) = \frac{1}{2} E_r \frac{\omega \omega_D}{\omega^2 + \omega_D^2} \tag{50}$$

so that we can compare against exact HEOM[60–64] dynamics. Here, $\omega_D = \omega^2/\eta$.

In Figures 7(a) and 7(b), we find that, in the site basis, SQCa with a quantum bath closely replicates not only the long time limit but also the correct transient dynamics in the site basis. In the excitonic basis, SQCa with a quantum bath gets the correct short time behavior, but the incorrect long time population. By contrast, SQCa with a classical bath correctly recovers the correct dynamics and the correct long time populations in the excitonic basis, but not in the site basis. Finally, in Figure 7(c), the temperature of the harmonic oscillators is plotted both at time zero and at the end of our simulation. It is clear that the quantum SQCa calculations are not leaking zero point energy from high to low frequency modes.

From these empirical observations, one can make several conclusions. First, SQCa with a quantum bath performs well in the site basis because of the consistent description of the nuclear quanta (not because of zero point leakage); short time SQCa dynamics with a quantum bath are an improvement over classical SQCa dynamics. Second, because there is no zero point leakage, it is very unlikely that our quantum SQCa simulations have reached equilibrium (unless the spin-boson model is truly non-ergodic). Third, until zero point leakage occurs through an equilibration of temperature, one cannot apply the classical arguments about partition functions and binning for the quantum SQCa data. Thus, there is no guarantee that quantum SQCa will necessarily recover the correct equilibrium electronic populations (even with small binning parameter in the excitonic basis). In the future, SQCa dynamics with a quantum bath should be studied in the framework of quasiclassical dynamics where there is a large body of literature on zero point energy effects, some studies focused on adiabatic dynamics[35,55–59] and others on nonadiabatic dynamics.[34,36] For instance, it would be helpful to study baths where zero point leakage can be modeled on reasonable time scales, so that energy flow from quantum to classical nodes can be explored in more detail.

Fourth, we must emphasize these dynamics are very difficult to simulate classically, and the overall performance of SQCa is impressive here. Even though FSSH nearly recovers the correct equilibrium populations in both the site and excitonic bases, note that FSSH slightly overestimates the rate slightly in the excitonic basis and drastically overestimates the rate in the site basis. Surface hopping dynamics fail in the site basis because the algorithm cannot accurately capture transient dynamics for long-lived coherences between wavepackets on different adiabatic surfaces. In other words, this is one example of the recoherence problem where the surface data and amplitude data will not agree, as wavepackets continuously separate and recombine.[46]

### C. The curse of "negative forces"

The last and most important item that must be addressed here is the question of "negative forces." Consider the PBME family of algorithms. These algorithms include ZPE through Eq. (8) and, as a result, there is the possibility of negative populations and, even more importantly, negative forces.[28–30,53,66] If one looks at Figures 1(c) and 1(e), one can already conclude that negative populations are present according to the amplitudes of PBME.

As is well known,[28–30,53,66] negative forces arise according to PBME because, according to Eq. (19), the final force is a weighted average of the individual forces, as weighted with populations $|c_1|^2 - \gamma$ and $|c_2|^2 - \gamma$

$$F_\sigma(\vec{x}) = (|c_1|^2 - \gamma) F_\sigma^1(\vec{x}) + (|c_2|^2 - \gamma) F_\sigma^2(\vec{x}). \tag{51}$$

Because $|c_1|^2$ and $|c_2|^2$ can approach zero for PBME, either of these populations can be negative, so that the final force can be the sum of one negatively-weighted force and one positively-weighted force. These negative forces must be considered a feature (rather than side-effect) of PBME dynamics because Bonella and Coker have shown PBME dynamics[29] can be considered a classical attempt to capture the quantum fluctuations around a stationary path integral; and in that framework, the classical path is simply the Ehrenfest path (with $\gamma = 0$) which is completely stable. In practice, however, these negative forces can lead to numerical instabilities.

Now, as demonstrated by Kelly *et al.*,[28] using the average force does help to alleviate some instabilities, i.e., there is an improvement in using

$$F_\sigma(\vec{x}) = \frac{1}{2}\left(1 + |c_1|^2 - |c_2|^2\right) F_\sigma^1(\vec{x}) + \frac{1}{2}\left(1 + |c_2|^2 - |c_1|^2\right) F_\sigma^2(\vec{x}). \tag{52}$$

However, even for PBMEa the final force can be the sum of one negatively-weighted force and one positively-weighted force.

In practice, we find that these instabilities are very minor for the spin-boson models: Even with some negative weighting, the average forces in Eqs. (21) and (19) are still harmonic and bound. However, for anharmonic potentials, negative-weighted forces can cause those trajectories to explore areas of phase space that would normally be energetically inaccessible and even sometimes unbound, as has been found before.[29]

#### 1. Equilibrium populations

Given the destructive nature of negative forces on PBME dynamics, we would like to probe the effects of negative forces on SQC dynamics and learn about the effect of binning. Obviously, with binning, we cannot find negative equilibrium populations but, beyond positivity, it is not obvious how well SQC will perform. Recall the case of two coupled Morse potentials (Eq. (43)).[29] In Figure 6, we showed that, unless $\gamma$ is very small, two weakly coupled Morse potentials with identical minima will not have equal populations according to any flavor of the mean-field-like dynamics we considered. To quantify the errors we find in Figure 6, let us consider

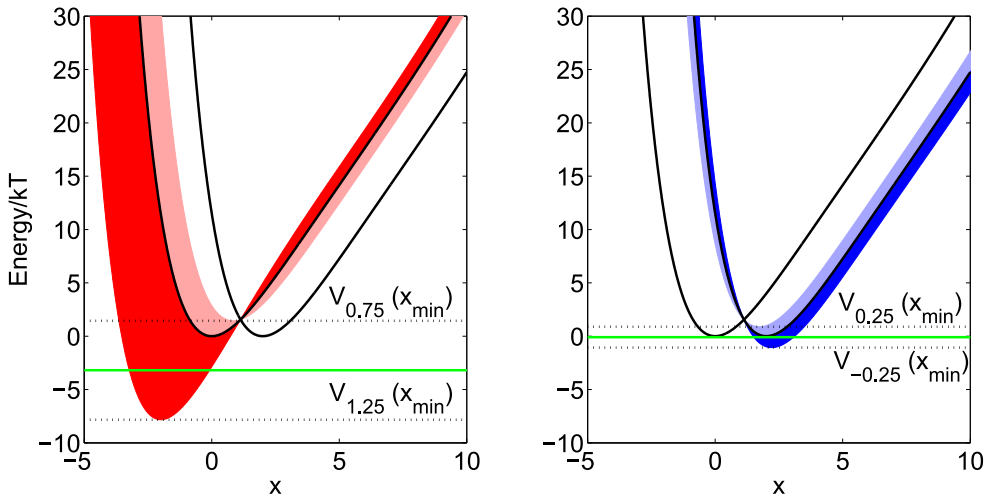


FIG. 8. The manifold of potential energy surfaces for mean-field trajectories within a window of $\gamma = 0.25$ (and $\alpha = 0.8$ in Eq. (41)). The red, pink, light, and dark blue areas map to regions of $V_\delta(x)$ from $\delta \in [1, 1.25], [0.75, 1], [0, 0.25]$, and $[-0.25, 0]$, respectively. The red and blue areas correspond to regions where one diabatic state feels a negative weight. Note that, in particular, the curves in the red shaded area can be far away from either of the original diabatic PESs. The dotted lines mark the minima of the wells at the edges of the window and the green lines denote the average of the minima. Notice that, by including a manifold of PESs, especially those with negative weights, an artificial driving force is introduced such that mean-field dynamics recover incorrect equilibrium populations.

the case where $\gamma = 0.25$ and $\alpha = 0.8$. For SQC dynamics, on average, $|c_1|^2 + |c_2|^2 = 1 + 2\gamma$. Thus, if the distribution of amplitudes were random, we could find $(|c_1|^2 - \gamma)$ and $(|c_2|^2 - \gamma)$ anywhere in the range of $[-0.25, 1.25]$. After windowing, we could find $(|c_1|^2 - \gamma)$ anywhere in the range of $[-0.25, 0.25]$ or $[0.75, 1.25]$ (and vice versa for $(|c_2|^2 - \gamma)$). In other words, our effective mean-field potential energy surface will be of the form

$$V_\delta(x) = \delta H_{11}(x) + (1 - \delta) H_{22}(x)$$
$$\delta \in [-0.25, 0.25] \cup [0.75, 1.25]. \tag{53}$$

Below, it will be useful to distinguish the cases of only positive weights, $\delta \in [0, 0.25] \cup [0.75, 1]$, versus the case of negative weights, $\delta \in [-0.25, 0] \cup [1, 1.25]$. In Figure 8, we color in red, pink, light blue and dark blue the windows of possible mean-field potential energy surfaces corresponding to the ranges $\delta \in [1, 1.25], [0.75, 1], [0, 0.25]$, and $[-0.25, 0]$, respectively. The minima of $V_\delta(x)$ for $\delta = -0.25, 0.25, 0.75, 1.25$ are drawn as dashed lines. Interestingly, even though the original anharmonic diabatic PESs have no driving force, including ZPE creates an artificial asymmetry.

The perspective in Figure 8 can be used to predict the incorrect equilibrium populations as given by SQC. In Figure 8, the solid green lines signify $\epsilon_1 = \frac{1}{2}(V_{0.75}(x_{min}) + V_{1.25}(x_{min}))$ (on the left) and $\epsilon_2 = \frac{1}{2}(V_{-0.25}(x_{min}) + V_{+0.25}(x_{min}))$ (on the right). In Figure 9, we plot SQC equilibrium populations versus the artificial function

$$f(\alpha) = \frac{1}{e^{-\beta(\epsilon_2(\alpha) - \epsilon_1(\alpha))} + 1}. \tag{54}$$

The behavior of $f$ tracks very well with the SQC data, suggesting that negative populations must be understood as a feature (rather than side effect) of these methods.

Lastly, for the SQCa method, we note that using an averaged surface (Eq. (20) instead of Eq. (18)) does dampen the effect of negative forces, and SQCa populations no longer match the function $f(\alpha)$ above. Nevertheless, negative forces are still present (even for the harmonic case, as one can also discern from Figure 1(e)). The fact that SQC and SQCa populations follow the same trend in Figure 9 is almost certainly the result of negative forces distorting the overall dynamics (and see below for more evidence).

### 2. Dynamics

Finally, we comment on the numerical instabilities caused by SQC when running dynamics. In Figure 10, we simulate the dynamics for two coupled Morse oscillators and plot population as a function of time. Without the ability to plot

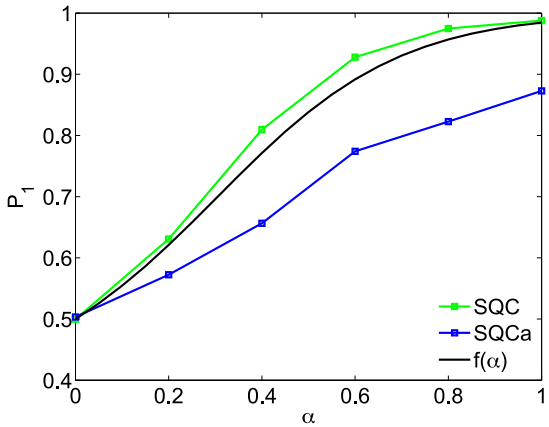


FIG. 9. The equilibrium populations as a function of increasing anharmonicity, $\alpha$, for the Hamiltonian in Eq. (41). Here, $\gamma = 0.25$. See Table I for a list of acronyms. Note that, if we apply windowing on top of PBME, the resulting SQC equilibrium populations still do not recover the correct answer for $\alpha = 1$ (two Morse potentials), $P_1 = 0.5$; instead, $P_1$ is close to 1.0. The incorrect mean-field results in this figure can be predicted using Boltzmann statistics on top of an artificial driving force caused by the existence of negative populations (Eq. (54), black line). Using the averaged force in Eq. (20) (for SQCa) (rather than Eq. (18) (for SQC)) helps, but SQCa populations are still unbalanced and suffer from negative populations.

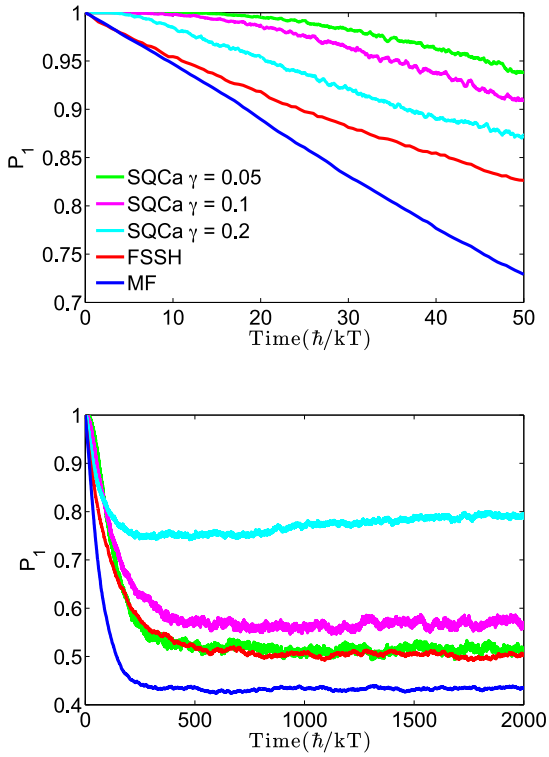


FIG. 10. The short and long time dynamics of the system of two morse oscillators described by Eq. (43) with $D_e = 20kT$, $a = 0.3$, $\lambda = 2$, $V_c = 0.2kT$, $m = 1$, and $kT = 5$. FSSH delivers the correct long time limit of $P_1 = 0.5$. Of the SQCa calculations, only $\gamma = 0.05$ recovers the correct long time limit $P_1 = 0.5$. Larger values of $\gamma$ were unstable due to the negative forces of the SQCa algorithm.

against exact data, we can compare between only surface hopping and mean-field approaches. Nevertheless, even by making such a limited comparison, we can learn a great deal about mean-field methods.

First, we observe that at SQCa displays different initial dynamics from FSSH and Ehrenfest. Second, at very long times, only FSSH and SQCa ($\gamma = 0.05$) go to the correct equilibrium value of $\frac{1}{2}$. Third, although not obvious from the figure, many trajectories become unstable for $\gamma \geq 0.25$: unstable trajectories run off to negative infinity, as they feel a negatively weighted repulsive Morse potential. For $\gamma = 0.1$ and 0.2, we require 10 000 trajectories for convergence; for $\gamma = 0.05$, we require 20 000 trajectories for convergence. Obviously, the ability to bin cannot eliminate the instabilities underlying mean-field results that include ZPE.

## V. CONCLUSIONS

We have dissected a host of inexpensive, mean-field mixed quantum-classical approaches for nonadiabatic dynamics–especially the SQC flavor of Cotton and Miller.[40] We find that the performance of these methods depends on the Hamiltonian, the binning parameter and the observable. In general, or at least for harmonic systems, the SQC ansatz of adding ZPE and binning the amplitudes represents a strong improvement over Ehrenfest dynamics. Moreover, for harmonic systems with strong electronic coupling, SQCa can give the correct dynamics in some cases where surface hopping fails completely. Regarding long time populations and detailed balance, we have shown that SQCa is guaranteed to recover the correct equilibrium population when (i) we apply the binning procedure in a diabatic basis with weak electronic coupling and (ii) we take the bin size to be very small ($\gamma \to 0$). Our findings about detailed balance extend previous results by Cotton and Miller for parallel surfaces.[54]

That being said, the reader should bear in mind that: (i) In order to sample enough different initial conditions to achieve branching, the $\gamma$ value cannot be too small. Thus, there are contradictory demands on the parameter $\gamma$ and SQC dynamics will work best when and if an optimal intermediate value of $\gamma$ is possible. (ii) When running SQCa dynamics, it would seem most natural to work in such a weakly coupled basis where detailed balance is guaranteed with a small enough value of $\gamma$. However, if one insists on using SQCa dynamics for a problem with strong electronic coupling, we have shown one must be careful about the choice of classical vs. quantum initial conditions for a bath. With the correct bath conditions, SQC dynamics can perform quite well for harmonic systems. Future work with quantum initial baths will need to investigate the possibility of zero point energy leakage.

Lastly and most importantly, for anharmonic systems, we find that all algorithms including ZPE (PBME, SQC, etc.) can lead to very unphysical trajectories (much more so than Ehrenfest dynamics) with correspondingly strong numerical instabilities. Thus, our results agree with previous findings.[28,30,53] The binning procedure incorporated by the SQC approach cannot yet eliminate these instabilities. The ability to simulate coupled, realistic anharmonic systems (as would be found using *ab initio* electronic structure theory) will be an important challenge for these methods.

## ACKNOWLEDGMENTS

We thank David Reichman, Stephen Cotton, and William Miller for helpful conversations. This material is based upon work supported by the U.S. Air Force Office of Scientific Research (USAFOSR) PECASE award under AFOSR Grant No. FA9950-13-1-0157 and the National Science Foundation Graduate Research Fellowship under Grant No. DGE-1321851.

## APPENDIX: INITIAL WAVE FUNCTION COEFFICIENTS FOR STANDARD PBME

For PBME dynamics, the initial coefficients are usually chosen as

$$c_i = \sqrt{(GRN(N_i, \gamma))^2}\, e^{i\theta},$$

where

- GRN$(0, \gamma)$ indicates a random number chosen from a ground-state harmonic oscillator distribution ($\zeta_0$): $\zeta_0(z) = \frac{1}{\sqrt{2\gamma\pi}} e^{-z^2/(2\gamma)}$.
- GRN$(1, \gamma)$ indicates a random number chosen from a first-excited state harmonic oscillator distribution ($\zeta_1$): $\zeta_1(z) = \frac{2z^2}{\sqrt{(2\gamma)^3\pi}} e^{-z^2/(2\gamma)}$.

On average, the norm of the initial amplitudes is equal to $4\gamma$ on average. For standard PBME,[11,23] we set the parameter $\gamma = \frac{1}{2}$, so that the norm is 2 for a two-state model.

Note that, in the body of this manuscript, we have implemented Eq. (8) for PBME initial conditions as a matter of convenience (rather than using the standard form above for PBME initial conditions).


[1]J. C. Tully, J. Chem. Phys. **93**, 1061 (1990).
[2]S. Hammes-Schiffer and J. Tully, J. Chem. Phys. **101**, 4657 (1994).
[3]F. Webster, E. T. Wang, P. J. Rossky, and R. A. Friesner, J. Chem. Phys. **100**, 4835 (1994).
[4]T. J. Martinez, M. Ben-Nun, and R. D. Levine, J. Phys. Chem. **100**, 7884 (1996).
[5]M. Ben-Nun and T. J. Martinez, J. Chem. Phys. **112**, 6113 (2000).
[6]A. Kelly and T. E. Markland, J. Chem. Phys. **139**, 014104 (2013).
[7]Q. Shi and E. Geva, J. Chem. Phys. **119**, 12063 (2003).
[8]T. C. Berkelbach, T. E. Markland, and D. R. Reichman, J. Chem. Phys. **136**, 084104 (2012).
[9]X. Li, J. C. Tully, H. B. Schlegel, and M. J. Frisch, J. Chem. Phys. **123**, 084106 (2005).
[10]S. J. Cotton, K. Igumenshchev, and W. H. Miller, J. Chem. Phys. **141**, 084104 (2014).
[11]H. Kim, A. Nassimi, and R. Kapral, J. Chem. Phys. **129**, 084102 (2008).
[12]H. W. Kim and Y. M. Rhee, J. Chem. Phys. **140**, 184106 (2014).
[13]C. C. Martens and J. Y. Fang, J. Chem. Phys. **106**, 4918 (1997).
[14]A. Donoso and C. C. Martens, J. Phys. Chem. A **102**, 4291 (1998).
[15]R. Kapral and G. Ciccotti, J. Chem. Phys. **110**, 8919 (1999).
[16]S. Nielsen, R. Kapral, and G. Ciccotti, J. Chem. Phys. **112**, 6543 (2000).
[17]Q. Shi and E. Geva, J. Chem. Phys. **121**, 3393 (2004).
[18]S. Nielsen, R. Kapral, and G. Ciccotti, J. Chem. Phys. **115**, 5805 (2001).
[19]D. M. Kernan, G. Ciccotti, and R. Kapral, J. Phys. Chem. B **112**, 424 (2008).
[20]I. Horenko, C. Salzmann, B. Schmidt, and C. Schutte, J. Chem. Phys. **117**, 11075 (2002).
[21]J. C. Tully, Faraday Discuss. **110**, 407 (1998).
[22]A. D. McLachlan, Mol. Phys. **8**, 39 (1964).
[23]H. D. Meyer and W. H. Miller, J. Chem. Phys. **70**, 3214 (1979).
[24]G. Stock and M. Thoss, Phys. Rev. Lett. **78**, 578 (1997).
[25]W. H. Miller, J. Phys. Chem. A **105**, 2942 (2001).
[26]C. V. N. Ananth and W. H. Miller, J. Chem. Phys. **127**, 084114 (2007).
[27]A. Nassimi, S. Bonella, and R. Kapral, J. Chem. Phys. **133**, 134115 (2010).
[28]A. Kelly, R. van Zon, J. Schofield, and R. Kapral, J. Chem. Phys. **136**, 084101 (2012).
[29]S. Bonella and D. F. Coker, Chem. Phys. **268**, 189 (2001).
[30]S. Bonella and D. F. Coker, J. Chem. Phys. **122**, 194102 (2005).
[31]S. J. Cotton and W. H. Miller, J. Chem. Phys. **139**, 234112 (2013).
[32]L. Bonnet and J. Rayez, Chem. Phys. Lett. **277**, 183 (1997).
[33]G. C. S. Kimberly and S. Bradley, J. Phys. Chem. **98**, 3788 (1994).
[34]A. A. Golosov and D. R. Reichman, J. Chem. Phys. **114**, 1065 (2001).
[35]G. Stock and U. Mller, J. Chem. Phys. **111**, 65 (1999).
[36]U. Mller and G. Stock, J. Chem. Phys. **111**, 77 (1999).
[37]P. V. Parandekar and J. C. Tully, J. Chem. Phys. **122**, 094102 (2005).
[38]J. R. Schmidt, P. V. Parandekar, and J. C. Tully, J. Chem. Phys. **129**, 044104 (2008).
[39]N. Doltsinis, in *Quantum Simulations of Complex Many-Body Systems: From Theory to Algorithms*, edited by J. Grotendorst, D. Marx, and A. Muramatsu (Kluwer Academic Publishers, 2002), pp. 377–397.
[40]S. J. Cotton and W. H. Miller, J. Phys. Chem. A **117**, 7190 (2013).
[41]J. E. Subotnik and N. Shenvi, J. Chem. Phys. **134**, 024105 (2011).
[42]B. R. Landry and J. E. Subotnik, J. Chem. Phys. **137**, 22A513 (2012).
[43]A. Jain and J. E. Subotnik, J. Chem. Phys. **143**, 134107 (2015).
[44]P. Huo and D. Coker, J. Chem. Phys. **137**, 22A535 (2012).
[45]C. Y. Hsieh and R. Kapral, J. Chem. Phys. **137**, 22A507 (2012).
[46]B. R. Landry, M. J. Falk, and J. E. Subotnik, J. Chem. Phys. **139**, 211101 (2013).
[47]J. E. Subotnik, W. Ouyang, and B. R. Landry, J. Chem. Phys. **139**, 214107 (2013).
[48]B. R. Landry and J. E. Subotnik, J. Chem. Phys. **142**, 104102 (2015).
[49]U. Weiss, *Quantum Dissipative Systems* (World Scientific Publishing Company, 1993).
[50]A. Nitzan, *Chemical Dynamics in Condensed Phases* (Oxford University Press, USA, 2006).
[51]In practice, the calculations were preformed with Langevin dynamics with $\lambda = 2$ and $m = 1$.
[52]Curiously, QCICa (without any binning) does even better than SQCa; apparently, for this problem, binning the final variables would seem to hurt results.
[53]G. Stock and M. Thoss, Adv. Chem. Phys. **131**, 243 (2005).
[54]W. H. Miller and S. J. Cotton, J. Chem. Phys. **142**, 131103 (2015).
[55]S. Habershon and D. E. Manolopoulos, J. Chem. Phys. **131**, 244518 (2009).
[56]G. H. Peslherbe and W. L. Hase, J. Chem. Phys. **100**, 1179 (1994).
[57]W. H. Miller, W. L. Hase, and C. L. Darling, J. Chem. Phys. **91**, 2863 (1989).
[58]J. M. Bowman, B. Gazdy, and Q. Sun, J. Chem. Phys. **91**, 2859 (1989).
[59]G. Czakó, A. L. Kaledin, and J. M. Bowman, J. Chem. Phys. **132**, 164103 (2010).
[60]Y. Tanimura and R. Kubo, J. Phys. Soc. Jpn. **58**, 101 (1989).
[61]Y. Tanimura, J. Chem. Phys. **137**, 22A550-1 (2012).
[62]A. Ishizaki and G. R. Fleming, J. Chem. Phys. **130**, 234111 (2009).
[63]J. Strmpfer and K. Schulten, J. Chem. Theory Comput. **8**, 2808 (2012).
[64]J. Strmpfer and K. Schulten, J. Chem. Phys. **131**, 225101 (2009).
[65]The FSSH dynamics presented are calculated with 2000 trajectories, $dt = 0.02\hbar/kT$, and 7500 harmonic bath modes evenly distributed up to the largest frequency $1500\omega^2/\eta$ ($1500\omega_D$).
[66]Q. Shi and E. Geva, J. Chem. Phys. **120**, 10647 (2004).
[67]W. H. Miller, Adv. Chem. Phys. **25**, 69 (1974).
[68]J. J. Cotton and W. H. Miller, J. Chem. Theory Comput. **12**, 983–991 (2016).